J Solid State Electrochem (1997) 1: 17–35

ORIGINAL PAPER

John O'M. Bockris · Yongku Kang

The protectivity of aluminum and its alloys with transition metals

Received: 18 November 1996 / Accepted: 17 February 1996

Abstract The mechanism of the protectivity of aluminum and supersaturated aluminum alloys containing W, Mo, Ta and Cu has been investigated in chloride environments. The potential of zero charge (PZC) of the passive film was evaluated by a method based on impedance spectroscopy. The chloride ion adsorption on the passive film was measured by means of an in situ radiotracer technique. Constituents of the passive film as a function of depth were investigated by means of ex situ spectroscopic techniques including XPS, ISS and SIMS. The PZCs of the passive films of Al and Al alloys were calculated from the flatband potentials. A linear correlation between pitting potential and the PZC was found. Adsorption of the chloride ion on the Al-Ta surface starts at more anodic potentials than those of pure Al, and this shift is in agreement with the anodic shift of the PZC. A constant surface concentration of chloride ion was observed during the induction time for breakdown. A significant decrease of OH^- concentration in the passive film of Al and its alloys has been found after the passive film has undergone breakdown. The mole fraction of the alloying elements in the surface region of the passive film is ca. 1–8%. The adsorption of the chloride ion on the surface of the passive film is influenced by the anodic PZC shift, which varies with the alloying element. However, retardation of the chloride penetration into the passive film by blocking of the entry site by oxide ions of the alloying element controls the rate of breakdown.

Key words Protectivity · Potential zero charge · Flatband potential · Breakdown

J.O'M. Bockris (✉) · Y. Kang
Department of Chemistry, Texas A&M University,
College Station, TX 77843, USA

Introduction

Aluminum supersaturated with transition metals (ca. 10%) has been found to provide an anomalously high protectivity towards corrosion in chloride environments [1, 2]. Several models have been proposed to explain this protectivity.

Natishan et al. have found that the pH of zero charge (pH_{ZC}) of the alloying element oxides is correlated to the pitting potential [1–4]. These authors proposed that the protectivity of supersaturated aluminum alloys towards corrosion is due to a decrease of the pH_{ZC} of the passive film by means of alloying.

Moshier et al. found an enrichment[1] of the alloying elements in the passive films by means of XPS analysis [2, 5–7]. The authors suggest that the oxidized alloying elements in the passive films restrict the transport of aggressive anions through these films by the formation of barrier layers of alloying elements.

Smialowska et al. [8, 9] suggest that the rate-determining step for pitting corrosion is the establishment of a solution pH within the pits which allows active dissolution of the metal oxides. The solubility of the oxide at this pH determines the protectivity of the alloys. The solubilities of the oxides of the alloying elements were found to be less than that of aluminum oxide.

Bockris and Minevski suggested on the basis of XPS and SIMS studies that the passive film of Al consists of Al_2O_3, $Al(OH)_3$ and a certain content of AlOOH in fibril form [10]. The authors proposed that the chloride ion diffuses into the passive film via the AlOOH fibril. A Ta-containing species (e.g. Ta_2O_5) blocks entry of the AlOOH fibrils by the chloride ions.

[1] "Enrichment" for the surface concentration of the alloying elements is considered only in respect to the metal cations in the surface. In the present paper, the mole fraction of film constituents has been calculated taking into account the surrounding oxide ion so that enrichments in the surface compared with the bulk is small or zero

Davis et al. [11, 12] explained the protectivity of the Al-Ta and Al-W alloys in terms of an alleged concentration of the alloying elements near defects in the film at which the pitting corrosion is initiated. The oxides of the alloying elements are known to have a pH_{ZC} which is lower than that of aluminum oxide. In a neutral solution pH, this would mean that a defect near the surfacewould have a negatively charged surface, and hence chloride ion would be repelled from this important site.

None of these models of the protectivity of the supersaturated Al alloys have been confirmed. In the present study, the nature of the protectivity has been studied by a comprehensive series of electrochemical, radiochemical and spectrochemical studies.

Experimental

Electrodes

The aluminum electrode was prepared by means of vacuum deposition of a pure aluminum (Alfa, 99.999%) on polished silicon wafers. Aluminum alloys used in this study were Al-W, Al-Mo, Al-Ta and Al-Cu. These were prepared by Martin Marietta Laboratory (Denver, Colo). The alloys were deposited on polished Si wafers by means of an RF magnetron co-sputtering method. The concentrations of the alloying elements were ca. 8 at%, and the thickness was ca. 1 μm.

The Al and the Al alloys were cut, and the back and edge sides of the electrode were covered by epoxy resin. The electrical contacts to a Cu wire were made by means of silver epoxy. These electrodes were mounted on a Teflon holder.

Electrolytes

Solutions were prepared from deionized water of resistivity less than 12 MΩ cm and were made up with 0.275 mol/l of sodium tetraborate mixed with 0.15 M boric acid. The solution pH was 8.4. The chloride concentration was adjusted in the range 10^{-4}–10^{-2} mol/l by adding NaCl to the borate buffer solution. The solution was purged with argon gas (Airco, 99.995%) through the fritted glass gas bubbler for 30 min to reduce the oxygen concentration. During electrochemical measurement, argon gas was passed over the solution to minimize oxygen contamination.

Electrochemical measurements

Electrochemical measurements were performed by means of an EG&G Princeton Applied Research potentiostat (PAR model 273). The current changes with respect to potential and time were recorded by means of a Hewlett Packard X-Y-t recorder (model 7044B). The electrochemical cell used in the study was a conventional three-compartment cell. Aluminum and aluminum alloys were used as the working electrode. Pt gauze was used as a counterelectrode and saturated calomel electrode (SCE) as a reference electrode. The counter-electrode was separated from the working electrode compartment by means of a fritted glass disc. The reference electrode was connected to a Luggin capillary to minimize the IR drop and chloride contamination.

Impedance measurements

Impedance measurements were performed on anodically grown passive films on Al and Al alloys in 0.1 M K_2SO_4 with the use of a Solartron model 1250 Frequency Response Analyzer and Solartron model 1186 Electrochemical Interface. The passive films were all grown at 1.0 V (vs NHE) for 30 min in the same electrolyte. A small-amplitude sine wave modulation signal (10 mV rms) from the analyzer was applied to the potentiostat (Solartron model 1186), and the resulting a.c. current was analyzed. The phase shift and amplitude changes of the a.c. current gave real and imaginary impedance values. The resulting impedance data were converted to digital signals and transferred to an IBM PC computer through an IEEE-488 standard signal bus for further calculation.

Radiotracer measurements

The radiotracer method used in this study was a thin foil method developed in this laboratory. A description of the experimental setup and procedures has previously been published [13–15].

The Al and the Al-Ta alloy were directly deposited onto the glass scintillator in a manner similar to that described above. The thickness of the metal layer was ca. 1 μm. The glass scintillator was purchased from Nuclear Enterprises (Plaineview, N.Y., model NE901). The roughness factor was estimated by a method initiated by Zelenay [13]. Thus, a potentiostatic current was measured at the same potential and substrate, except that aluminum was deposited in the one case on an Si wafer and in the other case on a glass scintillator. The roughness factor for Al and the Al-Ta alloy was found to be ca. 30. Borate buffer of pH 9.2 consisted of 0.0125 M sodium tetraborate and 9.0×10^{-4} M NaOH. Chloride was labeled with ^{36}Cl (supplied by ICN Radiochemical). The radionucleide is a soft β emitter with energy 0.714 MeV and was diluted by means of non-labeled compounds. The specific activity was 2–5 Ci/mole.

Ex situ spectroscopic measurements

A PHI model 5500 ESCA system (Perkin Elmer) was used for XPS and ISS analysis. The analyzer chamber pressure was maintained at less than 1×10^{-8} Torr. The spectral acquisition, signal averaging, deconvolution of the spectrum, and peak area calculation were performed by means of a computer equipped with an appropriate software package.

In the XPS analysis, samples were irradiated with a monochromated Mg Kα X-ray source. The acquired spectrum was calibrated with a C 1s peak (284.6 eV). The depth analysis was carried out by sputtering the sample. A 4 kV Ar^+ ion gun (5×10^{-8} Torr Ar pressure) was used for sputtering the sample. The ion gun was rastered over the sample of area 0.5 cm × 0.5 cm to minimize the edge effects. The sputtering rate was ca. 10 Å/min.

ISS studies were carried out at the surface, which had been examined by means of XPS to compare the data. A $^3He^+$ ion gun with 2-kV energy beam was used as probe ion in this study. The scattering angle was 134.5°.

Negative SIMS studies were performed on a KRATOS/3M model 535BX at Advanced R&D (Lake Elmo, Minn.). A $^{40}Ar^+$ ion gun with 0.5-keV energy beam was used as primary ion.

The sensitivity of the elements for the XPS study was accepted to be that provided by the manufacturer of the instrument. Sensitivity factors of Al and O for ISS were calibrated from thermally grown aluminum oxide, whose composition was confirmed by XPS analysis. Sensitivity factors of Cu, Mo, Ta and W for ISS were calculated from the scattering cross sections of these elements.

The samples were prepared in a dry box filled with nitrogen gas. The passive films were grown in pH 8.4 borate buffer without chloride in solution. The changes of passive film composition with depth were examined before and after breakdown in chloride-containing borate buffer solution. After electrochemical experiments, the sample was thoroughly washed with deionized water, dried in an argon gas atmosphere overnight and then transferred to the vacuum test chamber.

Results

Electrochemical measurements of passive-film breakdown for Al and its alloys

The breakdown rates of Al and the Al alloys were measured in pH 8.4 borate buffer containing 0.01 M NaCl. Passive films were grown potentiostatically in borate buffer solution without chloride at 1.0 V (vs NHE) for 30 min. A predetermined amount of NaCl was then added into the solution to make a solution of 0.01 M, and the solution was purged with Ar for 30 min. After the purging, a given potential was applied and the current measured as a function of time. A typical current-time transient curve is shown in Fig. 1. The rate of the passive film breakdown (v_{bd}) was taken as the inverse of the time of breakdown (τ_{bd}).

$$v_{bd} = \frac{1}{\tau_{bd}} \tag{1}$$

The $\log(v_{bd})$ for the Al passive film as a function of the applied potential is shown in Fig. 2. It is shown that

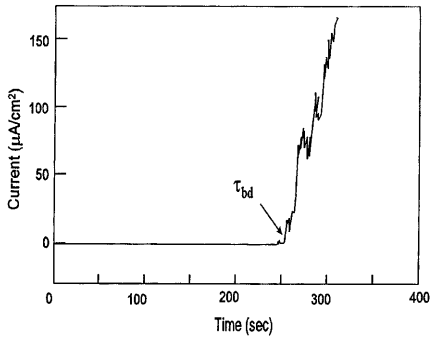

Fig. 1 Typical current-time transient curve for Al in pH 8.4 borate buffer, $[Cl^-] = 0.01$ M. Applied potential is −0.2 V vs NHE

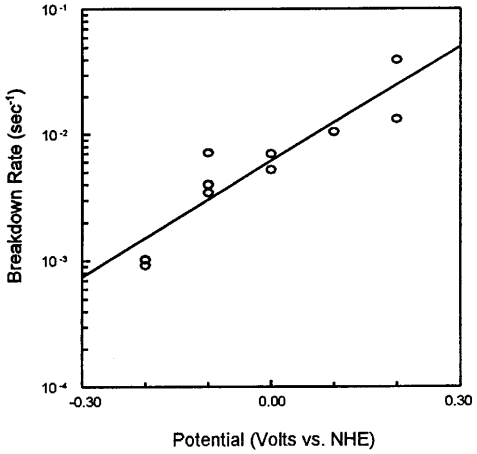

Fig. 2 Variation of the breakdown rate of Al as a function of the applied potential in pH 8.4 borate buffer containing 0.01 M NaCl

Table 1 Breakdown rates of the A1 and A1 alloy passive films

	A1	A1-Cu	Al-Ta	Al-Mo
$V_{bd}(s^{-1})$	0.69[a]	1.33×10^{-2}	2.98×10^{-3}	4.97×10^{-3}
Relative rate[b]	1	1.96×10^{-2}	4.38×10^{-3}	7.20×10^{-3}

[a] Estimated value from Fig. 2
[b] Relative rate compared with Al

$\log(v_{bd})$ linearly depends on the applied potential, the slope ($\delta \log(v_{bd})/\delta E$) being $2.84\,V^{-1}$.

Rates of passivity breakdown of the supersaturated Al alloys were measured at 0.6 V (vs NHE). Average breakdown rates are listed in Table 1. The breakdown rates of the Al alloys were ca. 100–200 times slower than that of the pure aluminum. The polarization curves for Al alloys in pH 8.4 borate buffer containing 0.01 M NaCl solution are shown in Fig. 3. The pitting potentials for the alloys were significantly shifted in the anodic direction compared to that of the pure aluminum. The pitting potential became more anodic in the sequence : Al < Al-Cu < Al-Ta < Al-Mo < Al-W.

Flatband potential measurements

The flatband potential (E_{fb}) can be determined by measuring the space charge capacitance (C_{sc}) with potential. The space charge capacitance is given by

$$\frac{1}{C_{sc}^2} = \left(\frac{8\pi}{\varepsilon e N_{sc}}\right)\left[E - E_{fb} - \frac{kT}{e}\right] \tag{2}$$

where ε is dielectric constant, N_{sc} is carrier density and E is applied potential. Thus, a plot of $1/C_{sc}^2$ versus E, a Mott-Schottky plot, gives a straight line. It is extrapolated to zero and the intersection on the potential axis gives the flatband potential (E_{fb}).

The semiconductor/solution interface under dark condition (majority carrier condition) has been modeled so that the surface states capacitance and space charge capacitance are placed in parallel (Fig. 4a) [16, 17]. However, this equivalent model has raised a number of difficulties in comparison with the requirements of the

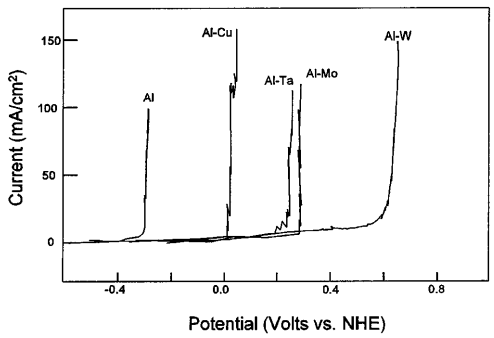

Fig. 3 Polarization curve for Al and Al alloys in pH 8.4 borate buffer, $[Cl^-] = 0.01$ M. Sweep rate = 1 mV/s

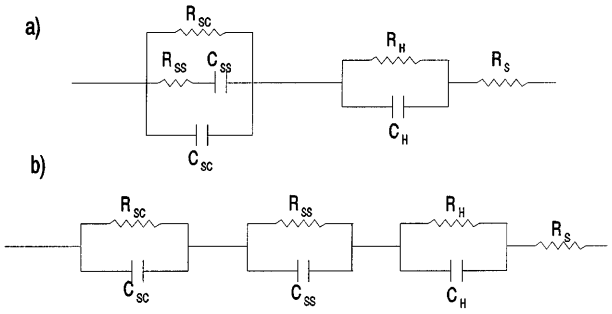

Fig. 4a, b Equivalent circuit models for passive film covered Al electrode: **a** conventional equivalent circuit; **b** equivalent circuit used in this study

Table 2 The estimated value for equivalent circuit components

R_H (Ω cm^2)	C_H (μF/cm^2)	R_{SS} (Ω cm^2)	C_{SS} (μF/cm^2)	R_{SC} (Ω cm^2)
5×10^3	50	5×10^5	18	560

real interface. Firstly, under d.c. conditions, electrons cannot pass through the surface states. Secondly, electrons can transfer from the bulk of the electrode to the surface states without passing through the space charge region, whereas it seems reasonable to have the electrons passing from the bulk of electrode into the space charge region, surface states and solution, and vice versa. Thus, the equivalent circuit for this semiconductor/solution interface was chosen to be as represented in Fig. 4b. Also, the semiconductor/solution interface under dark condition has been modeled with the space charge, surface states and Helmholtz layer in series. Each is a Warburg impedance. Similar equivalent circuits have been used for the semiconductor/solution interface [18, 19]. Knowing the equivalent circuit, the space charge capacitance can be numerically calculated when the other components of the equivalent circuit are known. The values of the equivalent circuit components were estimated by means of a semiempirical approach [20]. The estimated values of the equivalent circuit components are listed in Table 2.

Mott-Schottky plots of the passive-film-covered pure Al and its alloys are shown in Fig. 5. The plots show a linear relationship to applied potential. The Mott-Schottky plots show positive slopes. This indicates that the passive films of the Al and Al alloys are n-type semiconductors. Measured flatband potentials were found to be $-0.674, -0.514, -0.418, -0.317$ and -0.136 V (vs NHE) for Al, Al-Cu, Al-Ta, Al-Mo and Al-W, respectively. The carrier density of the passive film, which was calculated from the slope of the Mott-Schottky plot, was found to be ca. 5×10^{19} cm^{-3}.

Chloride adsorption and absorption on Al and Al-Ta surfaces

The surface coverages of the chloride ion on Al and Al-Ta surfaces were studied in pH 9.2 borate buffer solution containing NaCl. The chloride concentrations were 1.0×10^{-4}, 3.0×10^{-4} and 1.0×10^{-3} mol/l. The surface concentration-potential dependence curves of the Al and Al-Ta are shown in Figs. 6 and 7.

The surface concentration of chloride on Al starts to rise at ca. -1.5 V (vs NHE). The curve is sigmoidal. The maximum surface concentration (Γ_{max}) is reached at ca. -0.6 V (vs NHE). After reaching Γ_{max}, there is little further variation with potential. The potential dependence of the surface concentration of chloride on the Al-Ta surface was similar to that on Al. However, the surface concentration started to increase at ca. -1.1 V (vs NHE), and this potential was 0.4 V more positive than that of pure Al.

The dependence of the surface concentration on the chloride concentration at different potentials is shown in Fig. 8 for Al and Fig. 9 for Al-Ta. Both Al and Al-Ta showed a logarithmic dependence of the surface coverage on the solution concentration of the chloride (Temkin-type adsorption). The slopes ($\delta \log \Gamma / \delta \log c$)

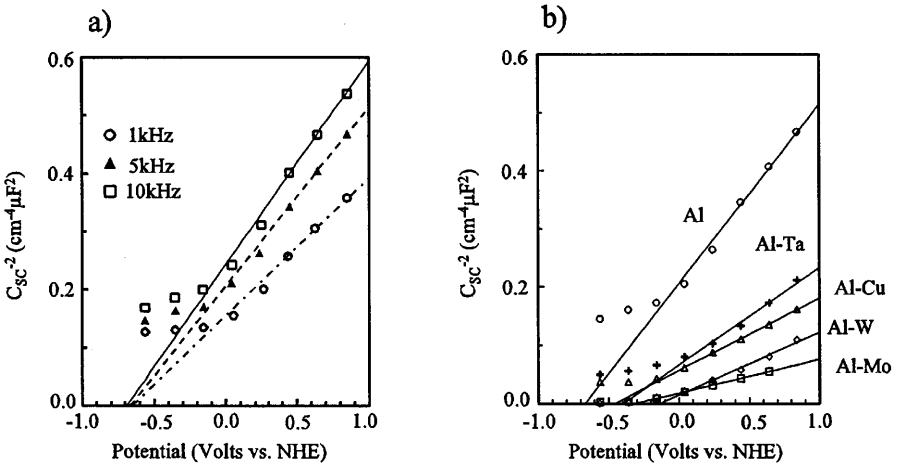

Fig. 5a, b Mott-Schottky plots for passive-film-covered Al and Al alloys: **a** frequency dependance for Al; **b** different Al alloys at a frequency of 5 kHz

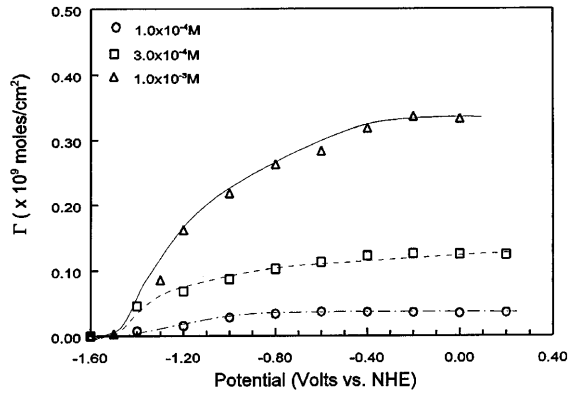

Fig. 6 Adsorption of the chloride ion on Al as a function of applied potential in pH 9.2 borate buffer containing different chloride concentrations. $[Cl^-] = 1 \times 10^{-3}$ M(Δ), 3×10 M (□), and 1×10^{-4} M (○)

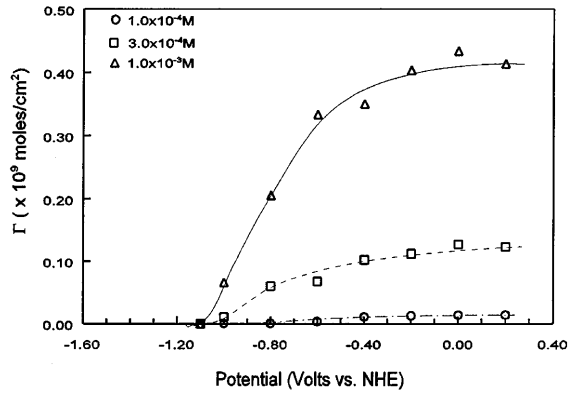

Fig. 7 Adsorption of the chloride ion on an Al-Ta surface as a function of applied potential in pH 9.2 borate buffer containing different chloride concentrations. $[Cl^-] = 1 \times 10^{-3}$ M(Δ), 3×10^{-4} M (□), and 1×10^{-4} M (○)

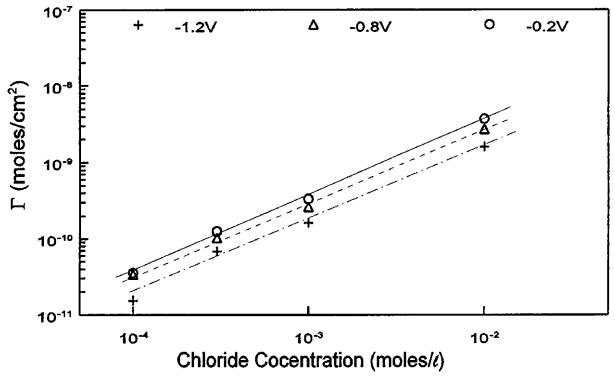

Fig. 8 Concentration dependence of chloride ion adsorption for Al in pH 9.2 borate buffer. Applied potential is −1.2 V(+), −0.8 V(Δ), and −0.2 V (○)

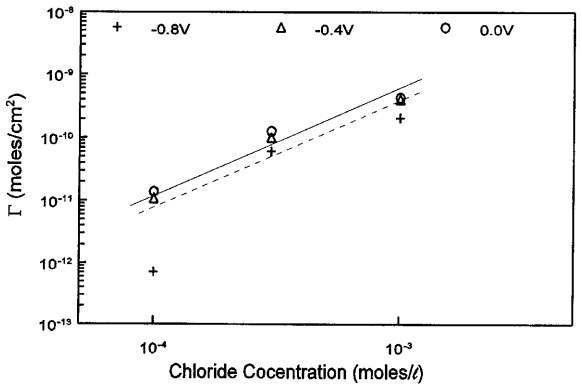

Fig. 9 Concentration dependence of chloride ion adsorption for Al-Ta in pH 9.2 borate buffer. Applied potential is −0.8 V(+), −0.4 V(Δ), and 0.0 V (○)

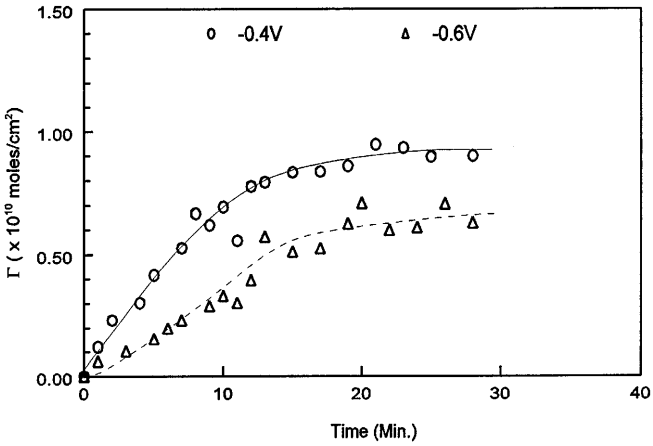

Fig. 10 Time dependence of chloride ion adsorption for Al-Ta in pH 9.2 borate buffer at applied potential of −0.4 V (○) and −0.6 V(Δ). $[Cl^-] = 3 \times 10^{-4}$ M

for Al were in the range 0.94–1.0 and for Al-Ta were in the range 1.45–1.56.

In Fig. 10, the time dependence of the surface concentration of the chloride on Al-Ta is shown in the presence of 3×10^{-4} mol/l chloride ion. The surface concentration of chloride reaches steady values after about 15 min for applied potentials of −0.4 V and −0.6 V (vs NHE). Thereafter, the surface concentration changes little with time when the applied potential is less than the pitting potential. However, if the potential is more positive than the pitting potential, the surface concentration abruptly increase with time after an induction time. The surface concentration of chloride and the corresponding current for Al-Ta in 0.01 M NaCl containing borate buffer is shown in Fig. 11. The applied potential was 0.5 V (vs NHE). The surface concentration reaches a plateau for the first 20 min. The surface concentration at this region was ca. 7×10^{-10} mol/cm^2. After this induction period, the surface concentration increases with time. The breakdown current increases in parallel with the surface concentration. The shape of the surface concentration transient curve is similar to that of the current transient. In Fig. 12, the surface concentration and current transient curves for pure Al surface is shown in 0.01 M

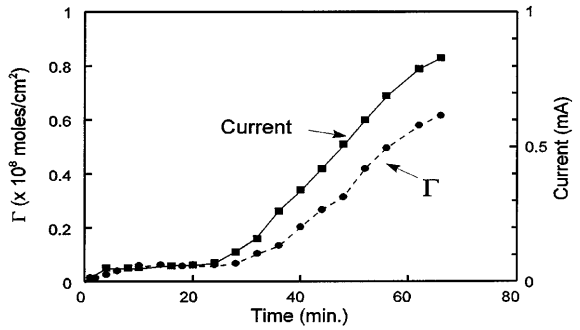

Fig. 11 Time dependence of surface concentration and current on Al-Ta in 0.01 M NaCl containing pH 9.2 borate buffer at applied potential of 0.5 V vs NHE: Γ (●) and current (■)

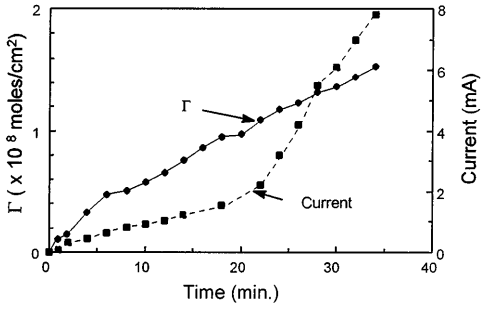

Fig. 12 Time dependence of surface concentration and current on Al in 0.01 M NaCl containing pH 9.2 borate buffer at applied potential of 0.2 V vs NHE: Γ (●) and current (■)

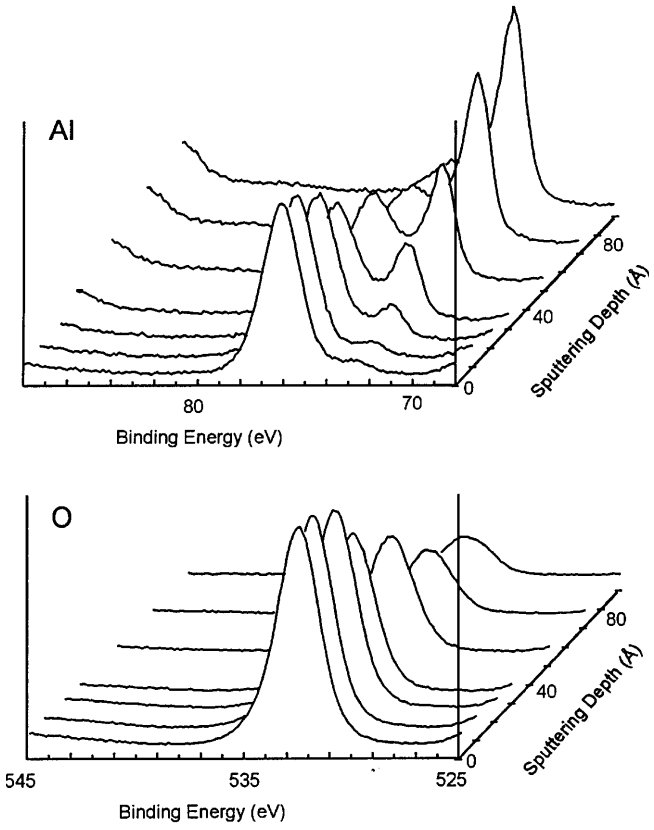

Fig. 13 Three-dimensional depth profile of Al passive film

NaCl containing a borate buffer. The applied potential was 0.2 V (vs NHE). The induction time for the Al was less than 2 min. This induction time for the pure Al is about 10 times smaller than that of the Al-Ta alloy. The surface concentration and current for an Al surface increases faster than that for an Al-Ta surface in this region. After the induction time, the slope for the surface concentration increase with time is 2.47×10^{-12} mol/cm^{-2}sec^{-1} for Al-Ta and 6.07×10^{-12} mol/cm^{-2}sec^{-1} for Al.

Ex situ spectroscopic measurements

A three-dimensional XPS depth profile of the passive-film-covered pure Al is shown in Fig. 13. The Al 2P peak has two peaks at about 72 eV and 75 eV, which correspond to metallic Al and oxidized Al (Al^{3+}) [21]. The relative intensity of the metallic Al peak gradually increases as a function of sputtering depth. The O 1S peak has a maximum at ca. 533 eV. The peaks does not show any appreciable shift as a function of sputtering. The O 1S peak was deconvoluted into two peaks, 531.6 eV and 533.3 eV. These peaks can be identified with oxygen in an aluminum oxide lattice (O^{2-} in Al_2O_3) and oxygen in hydroxyl [OH^- in $Al(OH)_3$, AlOOH or bound water] [21].

It has been shown that the metallic aluminum signal is due to the substrate aluminum (see Appendix). Thus, the atomic concentration profiles of the passive film constituents as a function of depth were calculated, neglecting the metallic aluminum signal intensity. The dependence of the passive film constituents of Al as a function of the sputtering depth is shown in Fig. 14[2]. The OH^- concentration decreases with increasing sputtering depth. The OH^- concentration at the surface is ca. 15 at% and sharply decreases to ca. 8% over the first 5 Å. After that, the OH^- concentration changes little with further sputtering. The $[O^{2-}]/[Al^{3+}]$ ratio is ca. 1.5 and remains almost constant in the passive film. The $[OH^-]/[Al^{3+}]$ ratio is 0.41 at the surface of the film. This ratio decreases to ca. 0.2 at a sputtering depth of 5 Å and changes only slightly with further sputtering.

Depth profiles of the passive film constituents for Al alloys are shown in Fig. 15. Concentration variations with sputtering depth of the Al^{3+}, O^{2-} and OH^- were similar to that of pure Al. The concentration of the alloying elements for passive films of Al-W, Al-Mo and Al-Ta at the surface region (0–15 Å) were ca. 5 at%. However, the Cu concentration in the passive film of Al-Cu at the surface was very small (about 0.1 at%). In

[2] The XPS signal intensity decreases exponentially with increasing depth, and ca. 64% of the signal intensity emanates within the depth of 16 Å from the surface of the sample. Therefore, if one makes, an approximation that the concentration of the passive film constituents is not varying within this depth range, the concentration being calculated here may be considered as the concentration of 8 Å below the sputtering depth

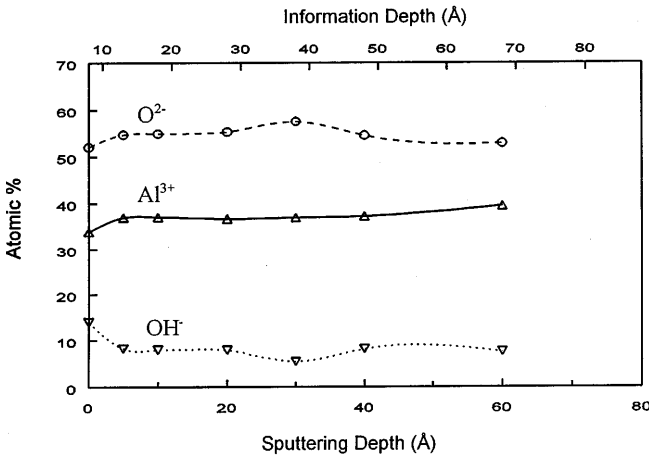

Fig. 14 XPS atomic concentration profile of the passive film of Al as a function of sputtering depth. Passive film formed in borate buffer at 1.0 V (vs NHE)

Fig. 16, the concentration variations of OH^- in the passive film of pure Al and its alloys before and after breakdown in chloride solution are shown. A significant decrease of the OH^- was observed after passive film breakdown.

Typical ISS spectra for pure Al and the Al alloy as a function of sputtering are shown in Fig. 17. The peaks can be seen at $E/E_o = 0.52$, 0.68 and 0.9, and correspond to oxygen, aluminum and alloying elements, respectively. The dependence of the [O]/[Al] ratio on the sputtering depth for Al passive film before and after breakdown is shown in Fig. 18. The [O]/[Al] ratio is ca. 1.95 at the surface of Al passive film and decreases with increasing sputtering depth. The [O]/[Al] ratio of the Al passive film reaches 1.5 after a sputtering depth of ca. 30 Å and changes little with further sputtering. The ratio in this range is close to the [O]/[Al] ratio for pure Al_2O_3. The variation of the [O]/[Al] ratio with sputtering depth for the passive film after breakdown is

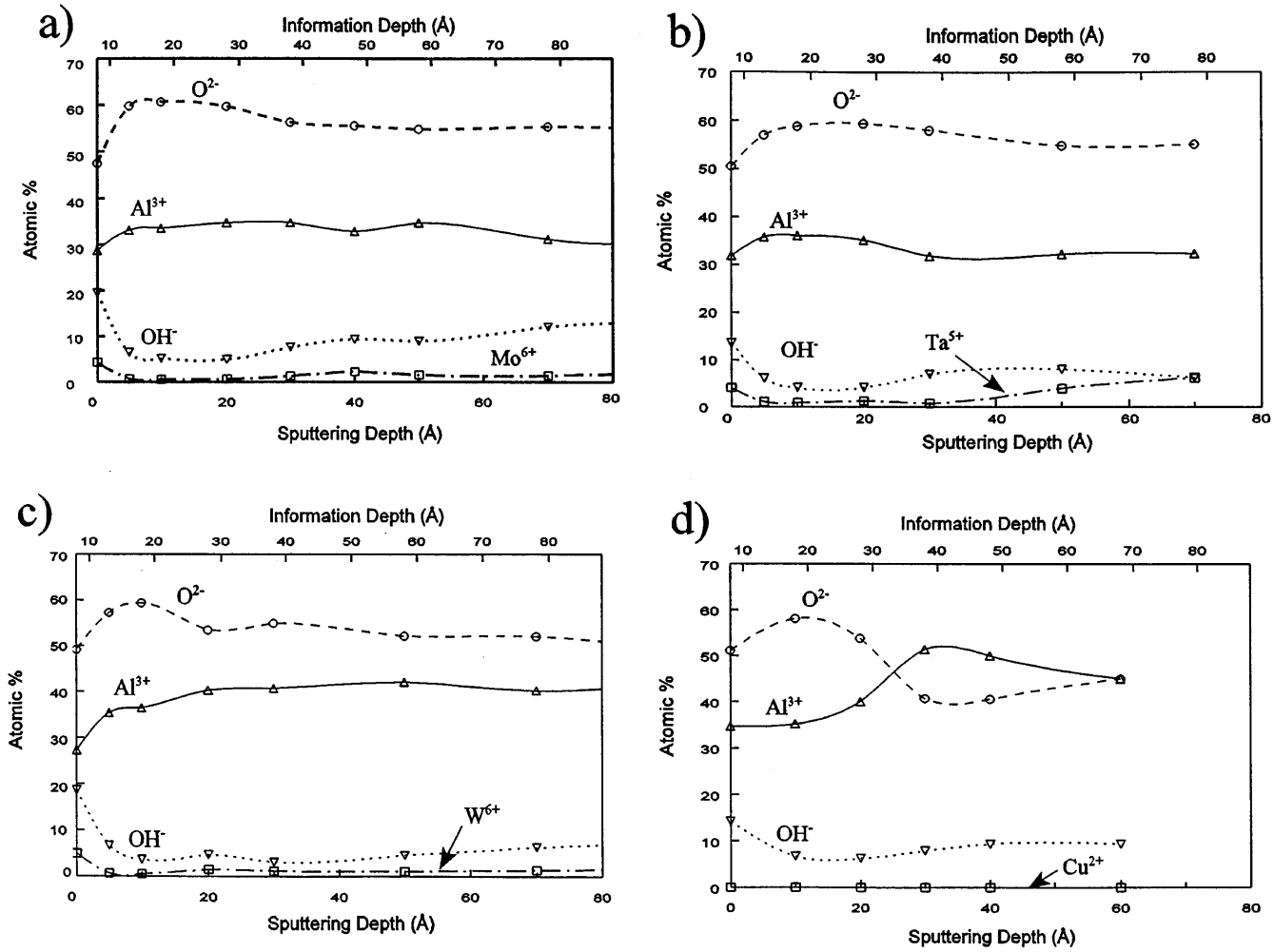

Fig. 15a–d XPS atomic concentration profile of the passive film of Al alloys as a function of sputtering depth: **a** Al-Mo, **b** Al-Ta, **c** Al-W, **d** Al-Cu. Passive film formed in borate buffer at 1.0 V (vs NHE)

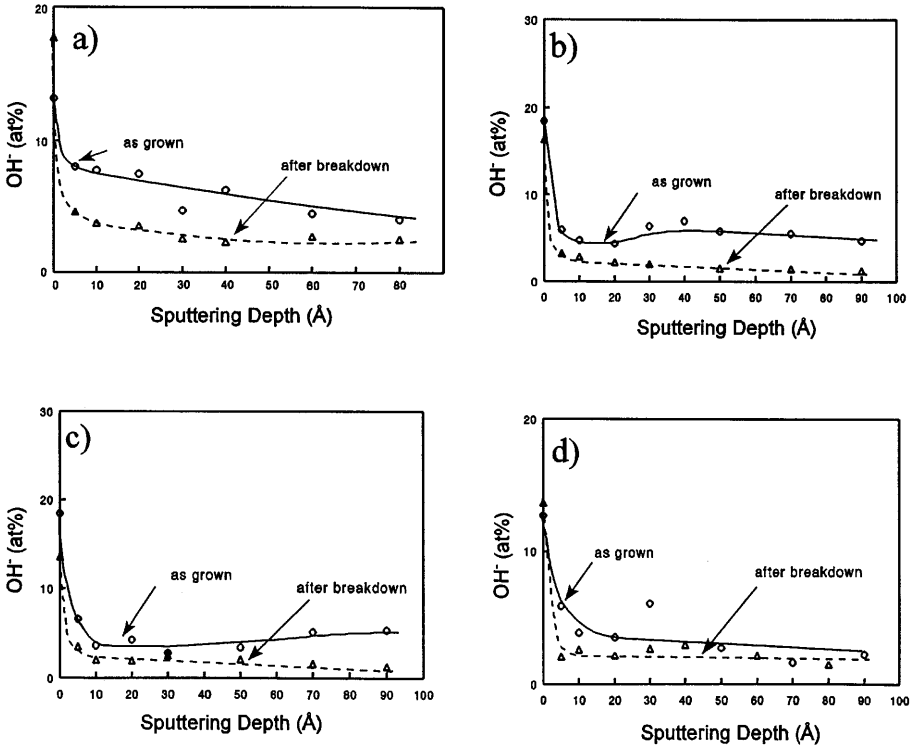

Fig. 16a–d Depth profile of the concentration of OH^- for Al and Al alloys: **a** Al, **b** Al-Mo, **c** Al-W, **d** Al-Ta

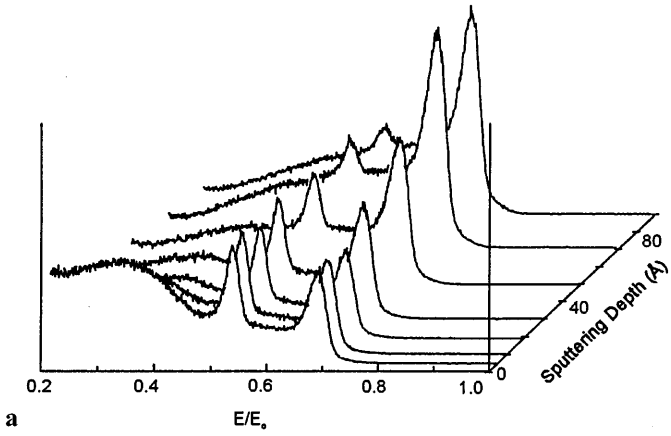

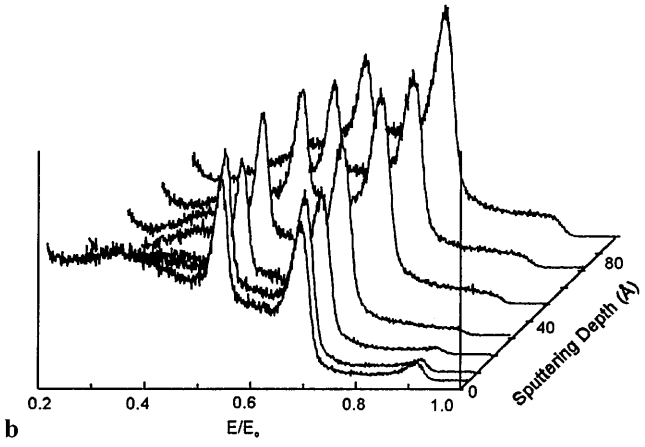

similar to that of the passive film before breakdown. However, the absolute values of the [O]/[Al] ratio are less after breakdown in the Al passive film. In Fig. 19, the atomic concentration of the alloying elements measured by means of ISS is compared with that measured by XPS. The concentrations of the alloying elements in the surface region of the passive film (0–15 Å) are ca. 2–3 times larger than that in the bulk of the passive film (15–60 Å). The concentration variation of the alloying elements measured by means of XPS is similar to that measured by ISS.

In Fig. 20, the ratios of [OH]/[O] measured by SIMS for Al and its alloys are compared with those measured by XPS. The XPS results are in good agreement with the SIMS results. The ratio in the surface region (0–1 Å) is ca. 0.45–0.5. However, this ratio decreases significantly to 0.15–0.25 at the depth of 10–15 Å and remains almost constant in the inner region of the passive film (15–60 Å). In the surface region, the passive film contains a relatively large concentration of OH^- that may be due to hydrated aluminum oxides such as $Al(OH)_3$ and AlOOH. The concentration of the hydrated aluminum oxides significantly decreases in the inner region of the passive film. Even though the concentration is small (5–7 at.%), OH^- still exists in the inner region. This result indicates that the inner layer of the passive film consists of aluminum oxide but also contains 5–7% of a hydrated oxide.

Fig. 17a, b ISS spectrum of passive film of **a** Al and **b** Al-Mo as a function of sputtering depth

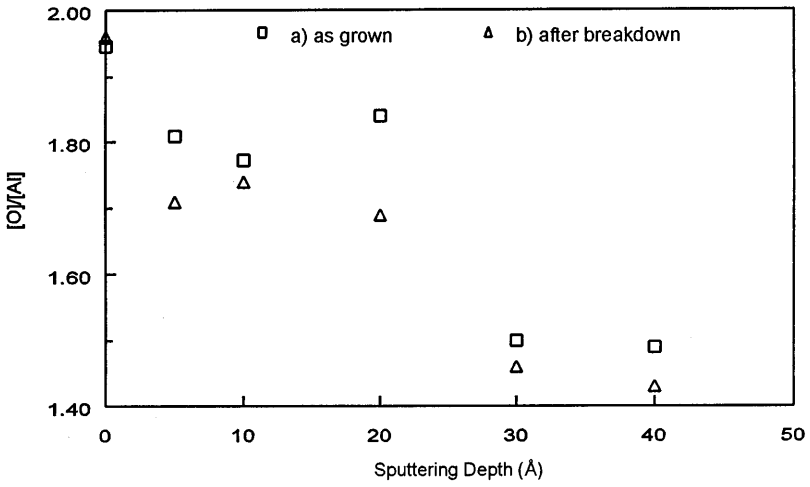

Fig. 18 The variation of [O]/[Al] ratio with sputtering depth for passive film of Al: **a** (□) as grown, **b** (Δ) after breakdown in 0.01 M NaCl

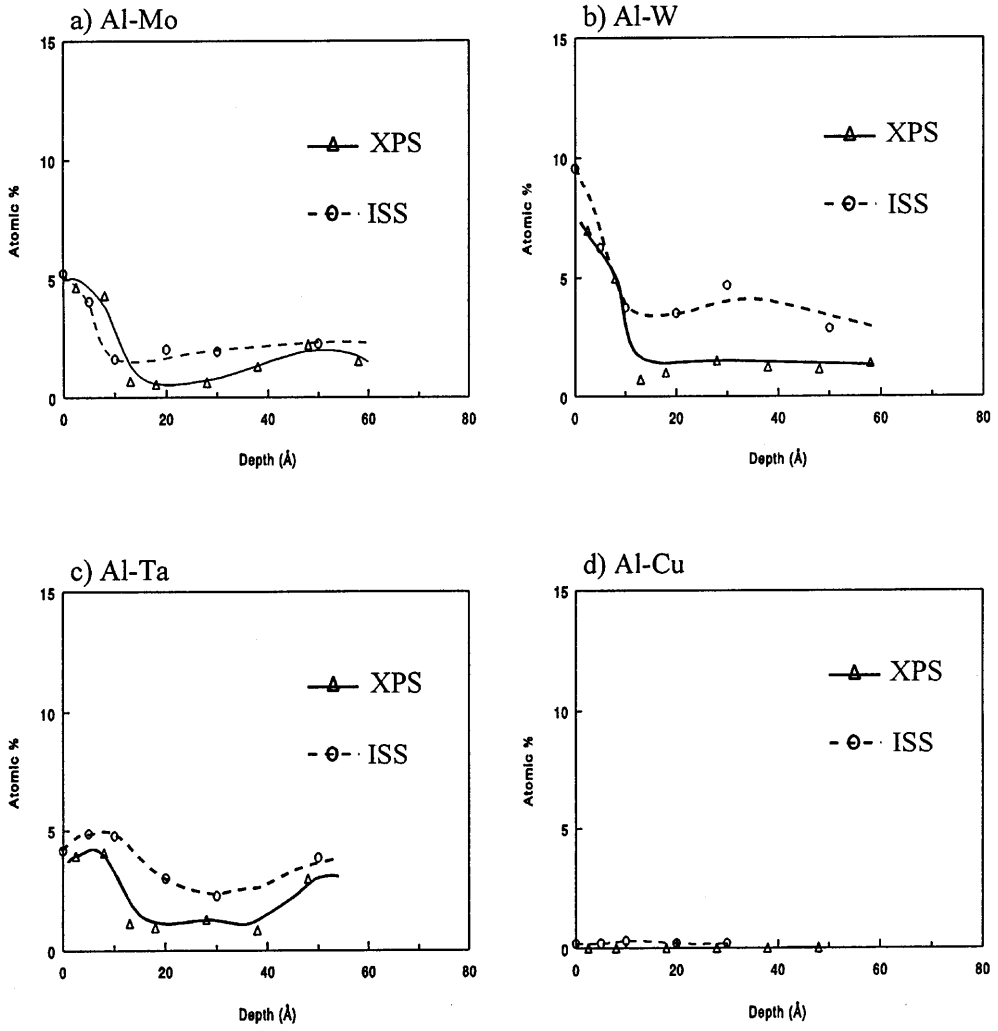

Fig. 19a–d The concentration of the alloying elements as a function of depth measured by means of XPS and ISS: **a** Al-Mo, **b** Al-W **c** Al-Ta, **d** Al-Cu

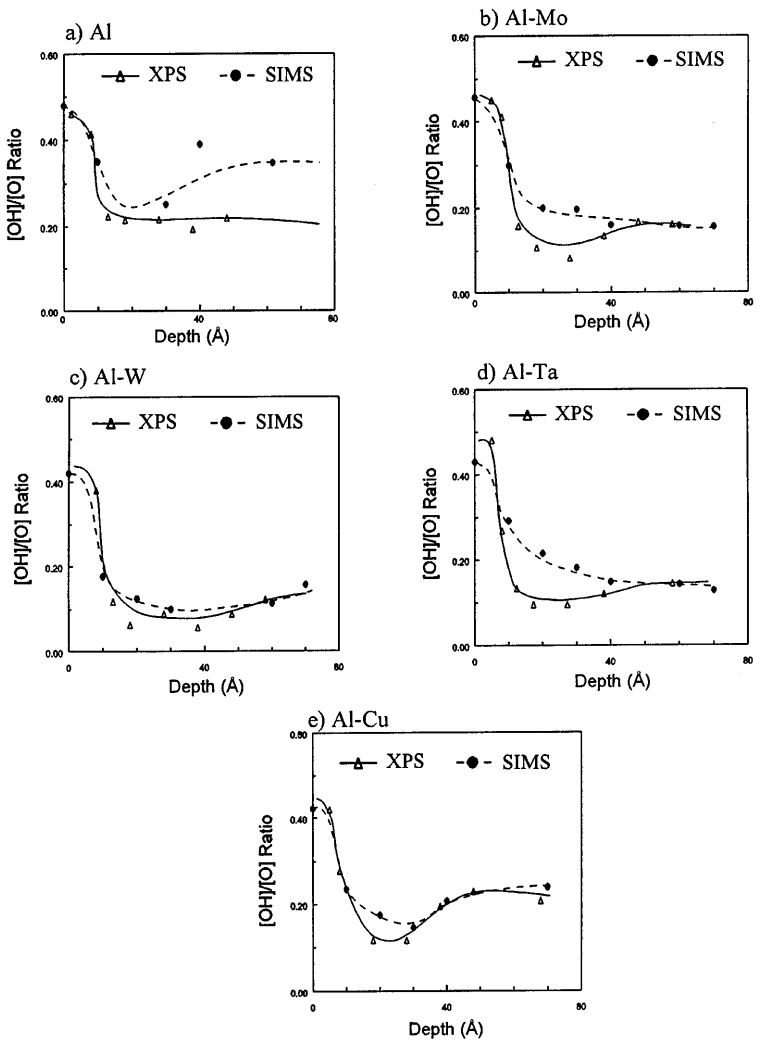

Fig. 20a–e The ratio [OH]/[O] as a function of depth measured by means of XPS and SIMS: **a** Al, **b** Al-Mo, **c** Al-W, **d** Al-Ta, **e** Al-Cu

Discussion

Flatband potential and PZC

Estimation of PZC from flatband potential

For the passive-film-covered metal electrode, the excess charge is distributed both on the surface of the electrode and in the space charge layer. At the flatband potential in the ideal case, if there is no specific adsorption, there is no potential drop across the space charge region. Correspondingly, the potential drop across the passive film/solution interface is negligible. Therefore, the flatband potential is the same as the PZC of the passive-film-covered metal electrode. However, specific adsorption must be considered for an actual passive-film electrode/solution interface. Thus, the potential drop across the Helmholtz layer is not zero at the flatband potential because of surface states induced by specific adsorption (Fig. 21). At the PZC, the charge density of the space charge layer (q_{SC}) must be equal to but opposite in sign to that of the surface states (q_{SS}), i.e. $q_{SC} = -q_{SS}$. Therefore, the PZC can be determined by the following equation when the potential drop of the space charge layer due to the specific adsorption is known.

$$E_{PZC} = E_{FB} \pm |\Delta\phi_{SC}| \tag{3}$$

where E_{PZC}, E_{FB} and $\Delta\phi_{SC}$ are the potential of zero charge, the flatband potential and the potential drop across the space charge layer, respectively. The potential drop across the space charge layer can be calculated from Eq. 4 [22] when the excess surface charge density (q_{SC}) is known.

$$q_{SC} = \left[\frac{\varepsilon N_{SC} kT}{2\pi}\right]^{1/2} \left[\exp\left(\frac{e\Delta\phi_{SC}}{kT}\right) - 1 - \frac{e\Delta\phi_{SC}}{kT}\right]^{1/2} \tag{4}$$

The most significant entities affecting the specific adsorption of the passive-film-covered electrode are H^+ (or OH^-) adsorption due to the acid-base reaction and chloride-specific adsorption.

The excess surface charge density due to acid-base properties of aluminum oxide depends on the pH_{ZC} and

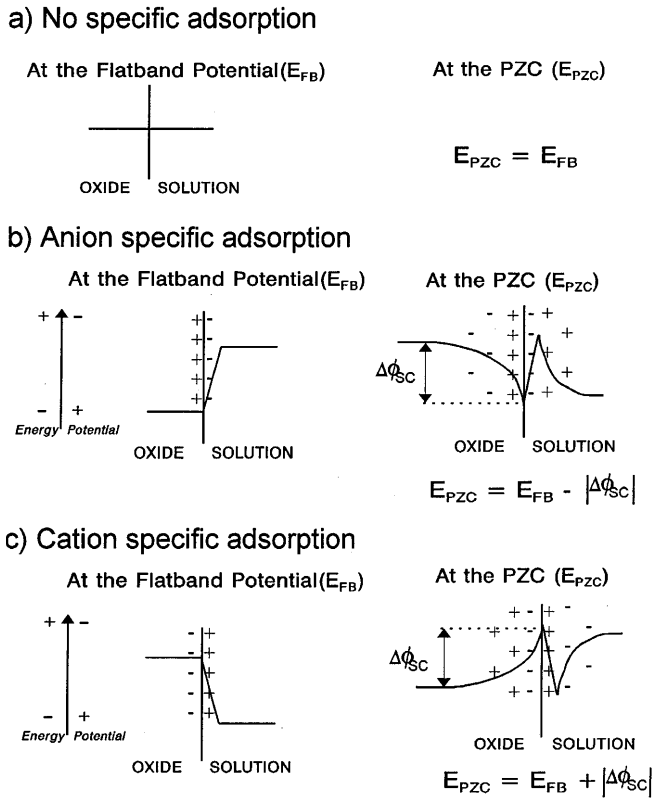

Fig. 21a–c PZC and flatband potential

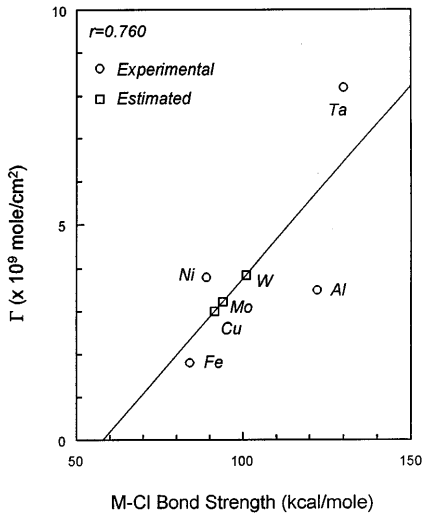

Fig. 22 Correlation between bond strength of M-Cl and surface concentration of chloride

hence the pH of solution and is known to be 2.0 $\mu C/cm^2$ per pH unit [23]. Thus, excess charge due to the acid-base property of the passive films can be calculated when the pH_{ZC} is known. The pH_{ZC} of the passive-film-covered Al and Al alloys can be estimated to a first approximation by the use of an ideal mixing equation:

$$pH_{ZC,alloy} = (1-f)pH_{ZC,AlOX} + f\,pH_{ZC,OX} \quad (5)$$

where f is the mole fraction of the alloying oxide in the passive film and $pH_{ZC,alloy}$, $pH_{ZC,AlOX}$ and $pH_{ZC,OX}$ are the pH_{ZC} of alloy, aluminum oxide and alloying element oxide, respectively. The mole fractions of the alloying elements oxide are estimated from XPS and ISS results. The mole fraction, pH_{ZC} of oxides, estimated $pH_{ZC,alloy}$ and excess charge density in the space charge layer (q_{SC}) due to acid-base properties of passive film are listed in Table 3.

The surface concentration of chloride on the passive films of Al and Al-Ta was measured in NaCl solution in this study (see Results), and that on Fe [15] and Ni [29] has been reported. The surface concentration of chloride on the passive films at the flatband potential is linearly correlated with the bond strength of metal-chloride (Fig. 22). Thus, the surface concentration of chloride ion on the passive films of the Al alloys could be estimated from the bond strength of metal-chloride and an ideal mixing law.

$$\Gamma_{Cl^-,alloy} = (1-f)\Gamma_{Cl^-,AlOX} + f\Gamma_{Cl^-,MOX} \quad (6)$$

where f is the mole fraction of the alloying oxide in the surface of the passive film of Alloy, $\Gamma_{Cl^-,alloy}$, $\Gamma_{Cl^-,AlOX}$ and $\Gamma_{Cl^-,MOX}$ are surface concentrations of chloride on the passive film of alloy, the passive film of aluminum and passive film of pure alloying element, respectively.

The potential drop across the space charge layer ($\Delta\phi_{SC}$) can be calculated from Eq. 4 for the estimated surface charge density. The determined flatband potential, the charge density of the space charge layer due to the solution pH ($q_{SC,acid\text{-}base}$) and the chloride adsorption (q_{SC,Cl^-}), the total charge density of the space charge layer ($q_{SC,total}$), the potential drop across the space charge layer ($\Delta\phi_{SC}$) and the estimated PZC from Eq. 3 are all listed in Table 4.

Table 3 Excess charge density in space charge layer (q_{SC}) due to acid-base properties of passive film in pH 8.4 solution

Oxides of	Mole fraction	$pH_{ZC,OX}$	$pH_{ZC,alloy}$	pH-pH_{ZC}	$q_{SC}(\mu C/cm^2)$	Ref.
Al	NA	8.6 (Al_2O_3)	8.6	−0.2	0.4	[24, 25]
Al-W	0.20	0.50 (WO_3)	6.98	1.42	−2.82	[25, 26]
Al-Mo	0.15	2.0 (MoO_3)	7.61	0.79	−1.58	[27]
Al-Ta	0.12	2.9 (Ta_2O_5)	7.92	0.48	−0.96	[28]
Al-Cu	0.01	9.5 (CuO)	8.61	−0.21	0.42	[25]

Table 4 PZC of passive-film-covered Al and Al alloys

	E_{fb} (Volts vs NHE)	$q_{SC,acid\text{-}base}$ $\mu C/cm^2$	q_{SC,Cl^-} $\mu C/cm^2$	$q_{SC,total}$ $\mu C/cm^2$	$\lvert\Delta\phi_{SC}\rvert$ (Volts)	E_{PZC} (Volts vs NHE)
Al	−0.674	0.4	−338.0	−337.6	0.331	−1.005
Al-Cu	−0.514	0.42	−338.0	−337.6	0.331	−0.845
Al-Ta	−0.418	−0.96	−392.0	−393.0	0.338	−0.756
Al-Mo	−0.317	−1.58	−334.0	−335.6	−0.330	−0.648
Al-W	−0.136	−2.84	−345.0	−347.8	0.333	−0.469

Table 5 Calculated work function of n-type metal oxide semiconductors

Passive films of	$E_{F,intrinsic}$ (eV)	Band gap energy (eV)	Work function of pure oxide (eV)	Mole fraction of alloy oxide	Work function of passive film
Al	−5.94	6.0	2.94 (Al_2O_3)	NA	2.94
Al-Cu	−5.96	1.4	5.16 (CuO)	0.01	2.96
Al-Ta	−6.31	4.6	4.01 (Ta_2O_5)	0.12	3.07
Al-Mo	−6.56	2.97	5.08 (MoO_3)	0.15	3.26
Al-W	−6.55	3.1	5.00 (WO_3)	0.20	3.35

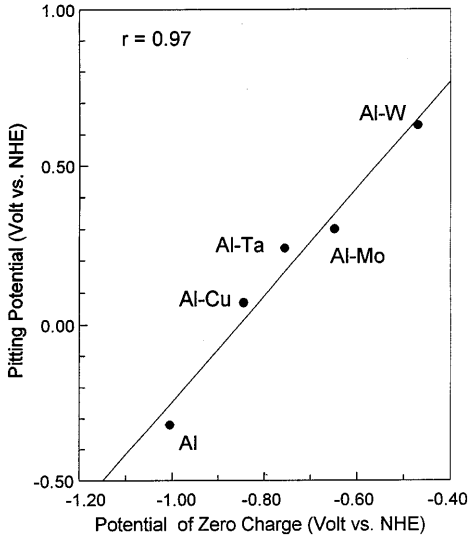

Fig. 23 Correlation between pitting potential and PZC

Correlation between PZC and pitting potential

The correlation between the determined PZC and the pitting potential is shown in Fig. 23. Thus, a linear relationship between pitting potential and PZC has been established. As the PZC of the passive-film-covered electrode shifts in a more anodic direction, the pitting potential also shift in the same direction. The adsorption of the chloride ion is strongly correlated with the applied potential and the PZC of the electrode. When the applied potential is more positive than the PZC, the surface of electrode has a net positive charge, and chloride ion is thus increasingly electrostatically attracted to the surface and adsorbed. The alloying element oxide in the passive film of the supersaturated aluminum alloy evidently shifts the PZC in a more anodic direction.

PZC and work function of the passive film

It is known that the PZC of the metal electrodes is linearly correlated with the work function [30, 31]. Thus, the change of the PZC of passive films can be estimated if the work function of the alloy passive film is known. The Fermi energy of an n-type semiconductor (E_F) can be expressed as [32]

$$-\Phi_{Oxide} = E_F \approx E_{F,Intrinsic} + \frac{1}{2}E_g \tag{7}$$

where $E_{F,Intrinsic}$ is the Fermi energy of the intrinsic semiconductor, and E_g is the bandgap energy. The Fermi energy of the intrinsic metal oxide semiconductor can be estimated [33–36] as the geometric mean of the atomic work function of the oxide constituents. Thus, the work function of the metal oxide has been calculated from the band gap energy of the semiconductor, the work function of the elements, and the mole fraction of alloying elements. The work function of the metal element, the calculated Fermi energy of the intrinsic metal oxide ($E_{F,Intrinsic}$), the band gap energy of the metal oxide, the calculated work function of the n-type metal oxide, the mole fraction of the alloying oxides, and the calculated work function of the alloy passive films are all listed in Table 5. A linear correlation between the calculated work function of the passive films and the PZC was found (Fig. 24). Thus, the anodic shift of the PZC of alloy passive films can be rationalized as the result of an increase in the work function of the passive films.

Chloride adsorption isotherm

A modelistic approach to the adsorption isotherm of inorganic ions on the electrode surface has been developed by Bockris et al. by utilizing the Floy-Huggins

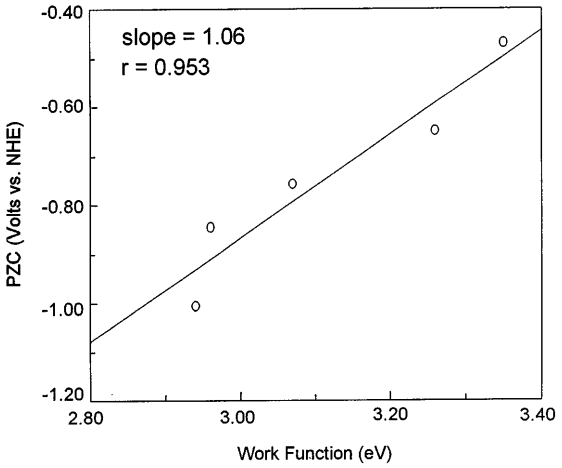

Fig. 24 Correlation between PZC and work function of the passive-film-covered Al and its alloys

isotherm and Nikitas's "uniform distribution" of adsorption energy [37]. The isotherm is given by[3]

$$\theta = \frac{1}{f}\left(-\frac{\Delta G^{o}_{Ch,i}}{kT} - \frac{\Delta G^{o}_{Ch,w}}{kT} - \frac{\Delta G^{o}_{E}}{kT} - \frac{\Delta G^{o}_{L}}{kT} + \frac{f}{2} + \frac{\mathrm{In}c_{ion}}{c_{w}}\right) \tag{8}$$

where f is a parameter related to the Nikitas's uniform distribution energy (U_o) and is defined as $f \equiv -2U_o/kT$, and $\Delta G^{o}_{Ch,i}$ and $\Delta G^{o}_{Ch,w}$ are standard free energies due to chemical interactions between the surface ion and surface water, respectively, ΔG^{o}_{E} is the free energy to bring an ion from the outer Helmholtz (OHP) to the inner Helmholtz layer (IHP), ΔG^{o}_{L} is the free energy change due to lateral interaction between adsorbed ions, c_{ion} is the concentration of adsorbate in the solution and c_w is the concentration of water in the solution. ΔG^{o}_{L} only depends on the surface coverage (θ). Thus, Eq. 8 can be written as:

$$f\theta + \frac{\Delta G^{o}_{L}}{kT} = a + \mathrm{In}c_{ion} \tag{9}$$

where $a = (-\Delta G^{o}_{Ch,i} - \Delta G^{o}_{Ch,w} - \Delta G^{o}_{E})/kT + f/2 - \ln(c_w)$.

A plot of $(f\theta + (G^{o}_{L}/kT)$ against $(\ln c_{ion})$ gives a straight line with unit slope. Thus, f can be obtained form Eq. 9 when ΔG^{o}_{L} is known. However, ΔG^{o}_{L} can be calculated from the surface coverage [37]. The details of this calculation for the chloride on the Al and Al-Ta surface has been reported elsewhere [20]. The factor f is determined by changing its values until the slope of Eq. 8, $\delta(f\theta + \Delta G^{o}_{L}/kT)/\delta(\ln c_{ion})$, is unity. In Fig. 25, the fitted plots of $(f\theta + \Delta G^{o}_{L}/kT)$ against $(\ln c_{ion})$ for adsorption of chloride on the passive layers of Al and Al-Ta are shown. The best fit f value was ca. 21 for both Al and Al-Ta surfaces. These results indicate that

[3]In this model, ΔG^{o}_{E} is a function of the charge density of the electrode and ΔG^{o}_{L} is a function of the surface coverage. Thus, these two terms are related to the electrode potential

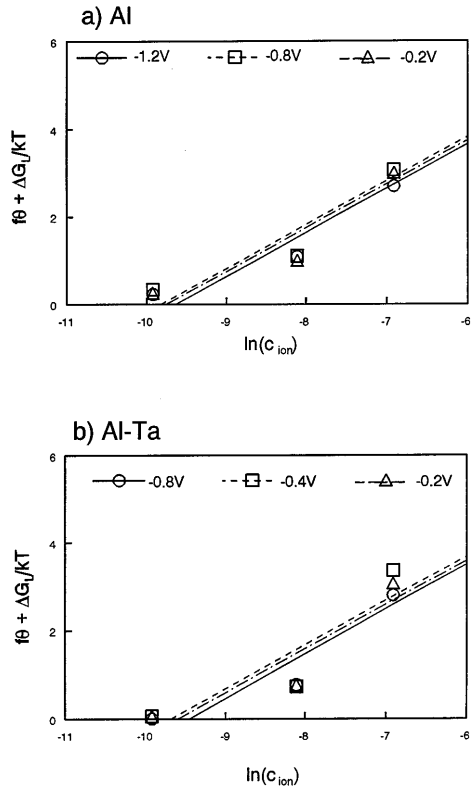

Fig. 25a, b Plots of $(f\theta + \Delta G^{o}_{L}/kT)$ against $(\ln c)$ for the adsorption of chloride on **a** Al, **b** Al-Ta

the modelistic isotherm using Nikitas's approximation [37] successfully represents the adsorption of chloride on Al and Al-Ta electrodes. The f value for chloride on a polycrystalline platinum electrode was reported to be 12 [38]. The f values of the chloride on the Al and Al-Ta determined in this study are larger than that on platinum. However, the f value of chloride on an aluminum electrode has been estimated using average surface M-M bond which is obtained from the Wolf-Klaproth equation [10]. The estimated f value of chloride on an aluminum surface was 27. The experimental f value in this study is reasonably matched by this estimated value.

The free energy of adsorption $\Delta(G^{o}_{ads})$ is expressed according to, $\Delta G^{o}_{ads} = \Delta G^{o}_{ch,i} + \Delta G^{o}_{ch,w} + \Delta G^{o}_{E} + \Delta G^{o}_{L}$. The lateral interaction energy (ΔG^{o}_{L}) can be determined from the measured surface coverage, and other interaction energies can be calculated form Eq. 10. Thus, ΔG^{o}_{ads} is given by

$$\Delta G^{o}_{ads} = \Delta G^{o}_{L} - kT(a - \frac{f}{2} + \ln c_{w}) \tag{10}$$

The calculated values of ΔG^{o}_{ads} for Al and Al-Ta at different potentials are listed in Table 6. The free energy of adsorption of chloride over the potential used in this study is -7.7 to -6.6 kJ/mol on Al and -6.9 to -5.3 kJ/mol on Al-Ta. These adsorption energies are similar to those measured for chloride adsorption on a passive-

Table 6 Free energy of adsorption of chloride on Al and Al-Ta

	Al			Al-Ta		
	1.2 V	−0.8 V	−0.2 V	−0.8 V	−0.4 V	−0.2 V
a	9.664	9.722	9.831	9.504	9.700	9.616
p	20.5	20.5	20.5	20.6	20.6	20.6
$\Delta G^{o}_{L}/kT$	0.307	0.612	0.852	0.433	1.083	1.182
$-\Delta G_{ads}$ (kJ/mol)	7.74	7.40	6.61	6.91	6.50	5.33

film-covered iron electrode which were reported to be −13.5 to − 18.5 kJ/mol [15].

Structure of the passive film

The XPS studies reported in this study show that the OH^- concentration in the passive film of aluminum strongly depends on the depth of the film. The concentration of the OH^- at the surface region of the passive film (0–15 Å from solution/passive film interface) is 15–20%. However, the concentration of OH^- in the inner region (15–60 Å) significantly decreases and is ca. 5%. The ISS studies show that the [O]/[Al] ratio is 1.8–2.0 at the surface region (0–20 Å), and then the ratio significantly decreases to 1.5 in the inner layer of the passive film (20–40 Å). The SIMS study also indicates the decrease of the [OH]/[O] ratio from ca. 0.5 to 0.25 in the thickness range of 0 – 15 Å.

The passive film of aluminum is known to be not a simple aluminum oxide but to be composed of a mixture of aluminum oxides and hydrated aluminum oxides [39, 40]. Utilizing spectroscopic techniques, it has been found that the passive film of aluminum is composed of a two-layer structure, with an amorphous hydrated outer layer and a dense inner layer between the amorphous outer layer and the metal [10, 41–43]. The probable composition of the outer layer is a mixture of Al_2O_3 and hydrated Al_2O_3 such as $Al(OH)_3$ and Al-OOH. However, the inner layer is mostly composed of Al_2O_3 and small amounts of hydrated aluminum oxide. Recently, the appearance of AlOOH in the aluminum passive film has been shown by X-ray absorption spectrum studies [44–46]. It is suggested that the Al-OOH can also exist in the inner layer of the passive film and this AlOOH can align itself into polymeric groups or fibrils (chain-like structures) [10, 47]. Thus, the structure of the inner layer of the aluminum passive film is composed of Al_2O_3 linked to the polymeric chain of AlOOH groups.

The ex situ spectroscopic results are consistent with the two-layer model. The structure of the passive film of aluminum can be qualitatively represented as Fig. 26.

The AlOOH fibril concentration in the Al and Al alloys can be estimated from the OH^- concentration in the inner layer of the passive film. If one assumes that the density of the passive film is the same as that of pure Al_2O_3, the density of the fibril is estimated to be

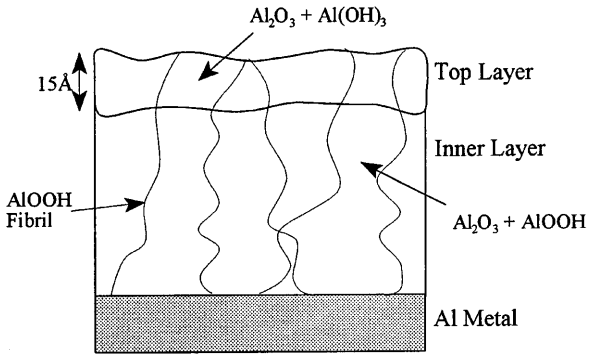

Fig. 26 The structure of the passive film of aluminum

$2.3 \times 10^{14}\,cm^{-2}$, $2.2 \times 10^{14}\,cm^{-2}$, $1.6 \times 10^{14}\,cm^{-2}$, $1.8 \times 10^{14}\,cm^{-2}$ and $1.4 \times 10^{14}\,cm^{-2}$ for passive films of Al, Al-Cu, Al-Ta, Al-Mo and Al-W, respectively. Thus, significantly, the density of the fibril decreases with the increase of the protectivity of the alloys.

Built-in electric charge

A possible electric charge in the passive film due to non-stoichiometry can be calculated when the concentrations of the passive film constituents are known. The built-in charge density (q, coulomb/cm^2) in the passive film can be obtained as follows:

$$q = \Sigma n_i z_i F \tag{11}$$

where n_i is concentration of passive film constituents (mol/cm^2), z_i is the charge on the ionic constituents and F is Faraday's constant. The XPS study gives the atomic concentration of the film constituents, and thus the molar concentration (n_i, mol/cm^2) can be calculated as

$$n_i = f_i \times \Sigma n_j \tag{12}$$

where f_i is the atomic mole fraction of the film constituent and Σn_j is total atomic concentration (mol/cm^2) in the passive film.

The calculated charge in the aluminum passive film before and after breakdown is shown in Fig. 27. The passive film carries a more negative charge after the film has been broken down in chloride solution. The calculated charge for various alloys is shown in Fig. 28. The charge in the passive films of aluminum alloys are of the

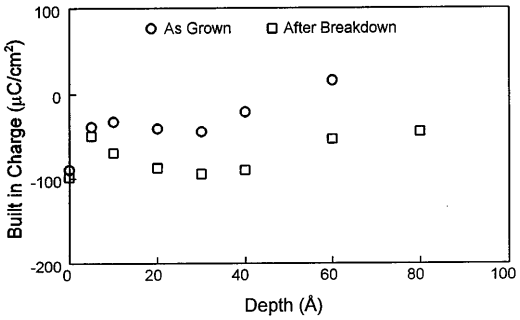

Fig. 27 Calculated built-in electrical charge for the passive film of aluminum as a function of depth

same order of magnitude as that of the pure aluminum passive film. The built-in charge is ca. 50–100 $\mu C/cm^2$. This value is similar to that reported by Bockris and Minevski [10].

However, the charge due to nonstoichiometry is compensated by the creation of charge-compensating defects such as high-valent cations or positively charged holes [48], and thus the net charge on nonstoichiometric oxides is seen as negligible. The concentration of charge-compensating defects is calculated to be ca. 2–5 mol% of the film, considered (as a first approximation) to consist of Al_2O_3. Such an interpretation must remain speculative because of the absence of detection of these entities in XPS.

Model of protectivity for supersaturated Al alloys

The main question for this study is how the small concentration of the alloying elements (ca. 8 at%) can enhance the protectivity ca. 100 times in a chloride environment compared to that of pure aluminum. In this section, several models will be proposed.

The breakdown of the passive film in the chloride environment involves the following steps [15, 49]: (a) adsorption of the chloride ion at the passive film-solution interface, (b) diffusion of chloride to the entry site, (c) chemical reaction of the adsorbed ion with materials at the entry site on the passive film surface, (d) penetration of the chloride ion into the passive film, (e) reaction of the chloride ion with the underlying aluminum, (f) passage of an Al-Cl entity through the film to the solution.

The model of the protectivity of the aluminum alloys will involve all of these steps, but one will be rate-determining.

Comparison of the previously published protectivity models

It has been proposed that chloride adsorption can be prevented by a decrease of the pH_{zc} of aluminum alloys [1, 3, 4]. Thus, H^+ and OH^- are equal adsorbents on the electrode at pH_{zc}. If this condition of neutrality occurs at low pH values and the solution pH remains relatively

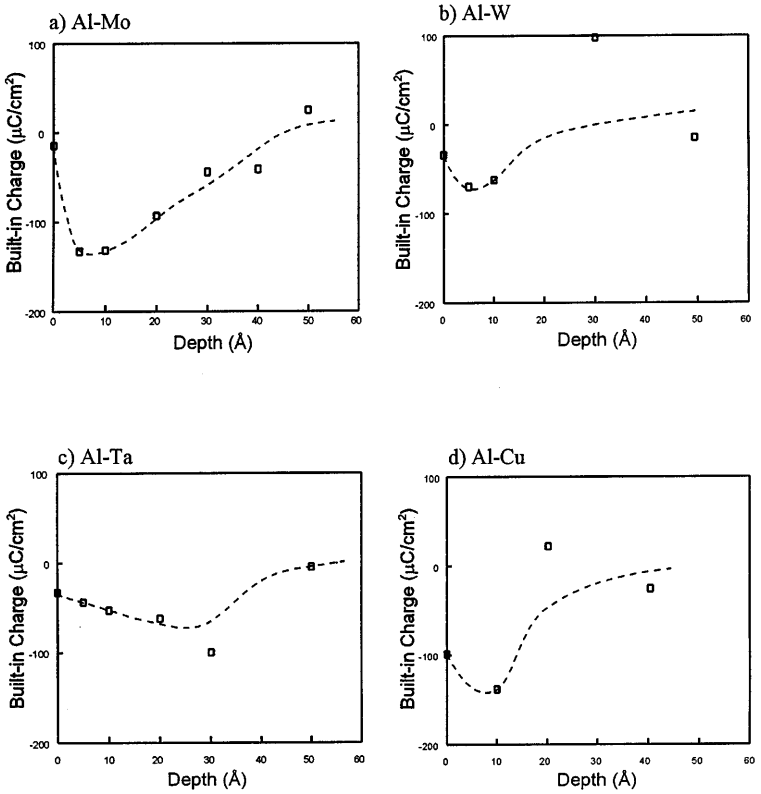

Fig. 28a–d The calculated built-in electrical charge for the passive films of Al alloys as a function of depth: **a** Al-Mo, **b** Al-W, **c** Al-Ta, **d** Al-Cu

high, an excess of OH^- ions adsorb on the electrode and therefore prevent the chloride adsorption. However, the electrode potential is a more important parameter in the control of the adsorption of the chloride ion than is the pH_{zc}. Moreover, it has been shown (see discussion of flatband potential and PZC and Table 3) that pH_{zc} change due to alloying is negligible (ca. 1 pH unit). Thus, the pH_{zc} cannot be the dominant parameter in the control of chloride adsorption.

An increase of alloying elements in the metal surface has been suggested as causing a decrease of pH_{ZC} near the defects [11, 12]. This is seen as happening because of the relatively rapid dissolution of aluminum, thus leaving behind a higher concentration of alloying element with lower pH_{ZC}. However, no increase of the alloying elements at the passive film/alloy interface has been found in our experiments (see ex situ spectroscopic measurements).

It is suggested the chloride penetration through the AlOOH fibril by means of a place exchange mechanism is the rate-determining step of passive film breakdown [10]. However, this model presents difficulties when one considers how the large chloride ion diffuses through the passive film.

Anodic PZC shift model

The first step of the passive film breakdown in a chloride-containing solution is the adsorption of chloride ion onto the surface of the passive film. The adsorption of chloride ions onto the surface of the film strongly depends on the electric charge of the electrode. An important parameter in determining the excess electrical charge at a given electrode potential is the PZC. If the applied potential is more anodic than the PZC, the electrode is charged positively and chloride ions can be easily adsorbed. However, if the electrode is more cathodic than the PZC, the electrode is charged negatively and the adsorption of chloride ions is largely prohibited (there is some specific adsorption).

It has been shown (see discussion of flatband potential and PZC and Fig. 23) that the PZCs of the passive film of aluminum alloys are shifted in a more anodic direction compared to that of the passive film of pure aluminum, and the PZC is linearly correlated with the pitting potential. Moreover, it has been shown (see discussion of flatband potential and PZC and Fig. 24) that the anodic shift of the PZC can be modeled by the work function variation of the passive film due to the alloying elements.

Therefore, the protectivity of the supersaturated aluminum alloy can be explained in terms of the adsorption of the chloride which would be retarded by the anodic PZC shift of the passive film due to the alloying elements.

Another aspect which one may consider is the electrical field change in the passive film due to the anodic PZC shift. The electrical field (V) in the passive film can be calculated by

Table 7 Calculated electrical field at 0.0 V (vs NHE)

Passive film of	E_{PZC}(Volts vs NHE)	Electrical field (V/cm)[a]
Al	−1.005	1.67×10^6
Al-Cu	−0.845	1.41×10^6
Al-Ta	−0.756	1.26×10^6
Al-Mo	−0.648	1.08×10^6
Al-W	−0.469	0.78×10^6

[a] The thickness of the passive film is assumed to be 60 A

$$V = \frac{E_{app} - E_{PZC}}{d} \tag{13}$$

where E_{app} is the applied potential, E_{PZC} is the potential of zero charge and d is the thickness of the passive film. The PZCs of the passive film and the calculated electric fields in the aluminum alloy passive films at 0.0 V vs NHE are listed in Table 7. The electrical field in the passive film of alloys, as exemplified by the electrical field in the passive film of Al-W, is about one half that of the passive film of pure aluminum at a given potential. Adsorbed chloride ions migrate into the passive film with the assistance of the electrical field [50]. Thus, the migration of the chloride into the alloy passive film may be retarded for the alloys because of the decrease of the electrical field within the passive film.

Therefore, the protectivity of the supersaturated aluminum alloys can be modeled according to the adsorption of the chloride and its change with the PZC of the alloys as well as the lessening of the electrical field within the passive film as a result of a shift of the PZC of the passive film.

Blocking the entry site model

One possible rate-determining step for the passive film breakdown in a chloride environment is the rate of the adsorbed chloride ion's penetration into the passive film. The surface of the passive film may be modeled as a non-uniform surface, and there may exist high energy sites (called special "entry sites") at which the chloride can be more strongly adsorbed and can subsequently penetrate into the passive film. The possible entry sites could consist of defects on the surface of the passive films such as dislocations, kink sites, grain boundaries and/or emergence points of the AlOOH fibril. One may speculate that the penetration rate of the chloride through one of these entry sites is faster than that at the other sites on the surface, and thus the rate of the passive film breakdown would depend upon the chloride ion penetrating through these entry sites only.

Richardson and Wood suggested that the possible entry site is an internal flaw which exists in the passive film [51, 52]. Recently, Bockris and Minevski proposed that the entry site is made of an AlOOH fibril which exits in the passive film [10]. Thus, the AlOOH fibril can

be considered as the crystal imperfection in the passive film. These crystal imperfections are mechanically stressed and may form small cracks (see Appendix).

It has been found that the surface energy of the passive film/solution interface decreases with the adsorption of chloride [53] and the critical stress for the extension of the crack may be reduced in the presence of chloride ion. Thus, the chloride ion at the top of the fibril may thus cause the fracture of the passive film along the fibril and hence the formation here of cracks at this point. Once the crack is formed, chloride ions can easily penetrate through it into the passive film. Thus, the formation of the crack due to the chloride adsorption would be the rate-determining step of passivity breakdown.

During the formation of the passive film, oxidized alloying elements (Mo^{6+}, W^{6+}, Ta^{5+}) can diffuse into the solution/passive film interface region, and some of them may remain in the double layer region in the form of tungstate, molybdate and tantalate. These anions are more likely to be deposited at the crystal imperfection sites which act as the entry sites for the chloride ions because of the high surface energy. Thus, the top of the entry site may be blocked by the alloying oxides. The lattice energy of the oxides of the alloying elements has been found to be ca. 1.5–2 times that of aluminum oxide [54]. The surface energy of the alloying oxide is expected to be significantly higher than that of aluminum oxide, and thus the fracture of the passive film may be prohibited. Therefore, the protectivity of the supersaturated aluminum alloys can be modeled as the blocking of the entry site by the alloying oxides and the prohibiting of the formation of a crack, which is the rate-determining step of the chloride penetration.

Comparison of the protectivity models with experimental results

The ''anodic PZC shift'' model is in good agreement with the following experimental results:

(a) The potential dependence of the passive film breakdown rate. (b) Linear correlation between measured PZC and pitting potential. (c) Anodic shift of the potential of the chloride adsorption of the Al-Ta is in good agreement with the anodic PZC shift of the Al-Ta alloy passive film.

However, this model cannot explain why the rate of the passive film breakdown of Al-Ta is ca. 10 times as slow as that of pure aluminum at the same electrical field with respect to the PZC. The adsorption of chloride ion on the surface of the passive film is the primary and essential step of the passive film breakdown. The rate of passivity breakdown may be affected not only by the adsorption of the chloride but also by other steps in the mechanism which are related to the structure of the passive films, such as chloride migration or penetration, chemical reaction with chloride, dissolution etc. Thus, the structural effects have to be considered fully to understand the protectivity of the alloys.

The ''blocking the entry site'' model is in good agreement with following experimental results:
(a) a constant surface coverage of chloride ion during the induction time (Fig. 11), (b) increase of the protectivity of the various alloys under conditions in which the electrical field in the passive film is the same (Figs. 11 and 12), (c) the AlOOH fibril structure in the aluminum passive film, (d) decrease of the OH^- concentration after the breakdown of the passive film, (e) enhancement of the protectivity of the alloys even though there is a very small concentration of alloying elements in the passive film .

However, this model cannot predict the potential dependance of the rate of the passive film breakdown and the linear relationship between the PZC and the pitting potential.

These two models do not contradict but support each other. The ''anodic PZC'' model can predict the potential dependance of the passive film breakdown and the ''entry site'' model can predict the structural dependance of the passive film breakdown. Thus, the protectivity of the supersaturated aluminum alloys can be modeled by combining these two models.

Briefly, the protectivity of the aluminum alloys is greatly enhanced by the anodic shift of the PZC of the aluminum alloy passive film and by blocking the entry site of the chloride penetration by means of a deposition of alloying elements oxides. Thus, adsorption of the chloride on the surface of passive film as well as chloride penetration into the passive film of the supersaturated alloys are greatly retarded by the presence of the alloying element.

Conclusions

The rates of passive film breakdown of supersaturated aluminum alloys in chloride-containing solutions are ca. 100 times as slow as that of pure aluminum at constant potential with respect to the hydrogen scale. Correspondingly, the rates of passive film breakdown of alloys are ca. 10 times as slow as that of pure aluminum at constant electrical field with respect to the PZC.

A significant anodic shift of the PZC of the aluminum alloys has been found. The PZC shifts of alloys can be rationalized by changes of the work function of the passive film due to the alloying elements. The PZCs of aluminum and its alloys are linearly correlated with the pitting potential in the chloride solution.

The potential at which the chloride starts to adsorb on the Al-Ta surface is shifted by ca. 400 mV in the anodic direction compared to that of pure aluminum. This shift is in agreement with the anodic shift of the PZC. The surface concentration of chloride on the Al-Ta passive film is similar to that of pure Al when the potential is less positive than the pitting potential. The

heat of adsorption of the chloride on the surface of Al and Al-Ta was −6.6 to − 7.7 kJ/mol and −5.3 to − 6.9 kJ/mol, respectively. Adsorption energies depend little on the applied potential.

The structure of the passive film of aluminum is modeled as two layers. The top layer is composed of aluminum oxide and hydrated aluminum oxide, probably $Al(OH)_3$ together with fibril-like AlOOH. The inner layer consists mostly of aluminum oxide and small amounts of hydrated aluminum oxide, probably a fibril form of AlOOH.

The protectivity of the aluminum alloys is enhanced by the anodic shift of the PZC of the aluminum alloy passive film and by blocking the entry site of the chloride penetration by means of a deposition of oxides of alloying elements. The adsorption of the chloride ion on the surface of the passive film is influenced by the anodic PZC shift, which varies with the alloying element. However, retardation of the chloride penetration into the passive film by prohibiting the crack formation by blocking the entry site of the chloride seems to be the rate-determining step in the mechanism of the protectivity of the supersaturated aluminum alloys.

Acknowledgements The authors wish to express their thanks to Dr. John Sedricks of the Office of Naval Research for the grant No. N00014-89-J-1566, which supports around half of their studies. The trustees of the Welch Foundation are to be thanked for their support of the remaining studies under grant No. A-0740. They thank Dr. W.C. Moshier of the Martin Marietta Laboratory who prepared the Al alloys and Dr. G. Sparrow of the Advanced R&D Co. who carried out the SIMS measurements. They would also like to thank Dr. A. Gonzalez-Martin, Dr. M. Gamboa-Aldeco and Dr. L. Minevski for helpful discussions.

Appendix i: XPS metallic aluminum signal

For the thin passive-film-covered aluminum electrode with thickness d, the signal intensity due to the passive film for each element (I_j) can be expressed as follows:

$$I_j = S_j \sin\theta\, N_j(x) \exp\left(1 - \frac{d}{\lambda \sin(\theta)}\right) \tag{14}$$

where S_j is the sensitivity factor for element j, $N_j(x)$ is the number of atoms at a depth x, λ is the mean free path and θ is the take-off angle. The signal intensity due to aluminum substrate ($I_{Al(M)}$) also can be expressed as

$$I_{Al(M)} = S_{Al} \sin\theta N_{Al(M)}(x) \exp\left(\frac{d}{\lambda \sin(\theta)}\right) \tag{15}$$

Thus, the apparent atomic concentration of metallic aluminum due to the substrate can be calculated as follows

$$C_{Al(M)} = \frac{I_{Al(M)}/S_{Al}}{I_O/S_O + I_{Al(OX)}/S_{Al} + I_{Al(M)}/S_{Al}} \tag{16}$$

where I_O and $I_{Al(OX)}$ are XPS signal intensities due to oxygen and aluminum ions in the passive film, respectively, and S_O and S_{Al} are sensitivity factors of oxygen and aluminum, respectively. Thus, from Eqs. 16, 17 and 18, the apparent metallic Al concentration due to substrate ($C_{Al(M)}$) can be expressed as

$$C_{Al(M)} = \frac{N_{Al(M)} \exp\left(-\frac{d}{\lambda \sin(\theta)}\right)}{N_O \exp\left(1 - \frac{d}{\lambda \sin(\theta)}\right) + N_{Al(OX)} \exp\left(1 - \frac{d}{\lambda \sin(\theta)}\right) + N_{Al(M)} \exp\left(-\frac{d}{\lambda \sin(\theta)}\right)} \tag{17}$$

where $N_{Al(OX)}$ and N_O are the numbers of atoms in the passive film for aluminum and oxygen, respectively, and $N_{Al(M)}$ is the number of aluminum atoms in the substrate. The $N_{Al(OX)}$ and N_O can be obtained from the density of the aluminum oxide. Thus, the apparent metallic aluminum concentration can be calculated when the thickness of passive film (d), take-off angle (θ) and mean free path (λ) are known using Eq. 19. The take-off angle is 45° and the mean free path is ca. 20 Å in aluminum oxide.

The calculated apparent metallic aluminum concentration and experimental concentration as a function of the sputtering depth is shown in Fig. 30 when the thickness of the passive film is assumed to be 65 Å. The experimental apparent concentration of metallic aluminum concentration is in good agreement with the calculated concentration.

Appendix ii: Stress for critical crack formation

If one considers the AlOOH fibril as an inclusion in the Al_2O_3 crystal, the critical stress (σ_{crit}) for crack extension is given by Eq. 18 using the Griffith model [55]:

$$\sigma_{crit} = \sqrt{\frac{2Y\gamma}{\pi(1-\nu)h}} \tag{18}$$

where Y is Young's modulus, γ is the surface energy, ν is Poisson's ratio and h is the length of the crack. Young's modulus, surface energy and Poisson's ratio of aluminum oxide are given respectively as 3.6×10^{12} dyne/cm^2, 6000 dyne/cm and 0.26 [56, 57]. The length is assumed to be the same as the thickness of passive film, 60 Å. The critical stress is calculated to be 1.7×10^{11} dyne/cm^2.

The hydrostatic stress (σ_h) at an edge dislocation is given by [58]

$$\sigma_h = \frac{\tau b(1+\nu)}{3\pi(1-\nu)} \frac{\sin\theta}{r} \tag{19}$$

where τ is the rigidity modulus, b is Burger's vector, θ is the angle with respect to the glide plane, and r is the distance from the center of the dislocation. The rigidity modulus for aluminum oxide is given as 1.6×10^{12} dyne/cm^2 [58]. Taking $r \approx b$ and θ as 45°, the hydrostatic stress is calculated to be 2.0×10^{11} dyne/cm^2. Thus, the stress due to dislocations introduced by the presence of fibrils is of the same order of magnitude as the critical stress of the crack extension for the aluminum passive film due to the AlOOH fibril.

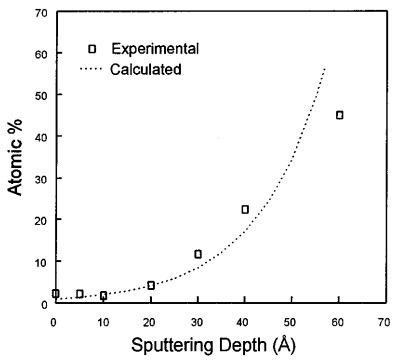

Fig. 29 Comparison between measured and calculated apparent metallic aluminum concentration in the passive film of Al

References

1. Natishan PM, McCafferty E, Hubler GK (1988) J Electrochem Soc 135:321
2. Shaw BA, Davis GD, Fritz TL, Rees BJ, Moshier WC (1991) J Electrochem Soc 138:3288
3. Natishan PM, McCafferty E, Hubler GK (1986) J Electrochem Soc 133:1061
4. McCafferty E, Natishan PM (1992) In: Frankel Gs, Newman RC (eds) Critical factors in localized corrosion. Electrochemical Society, p 299
5. Moshier WC, Davis GD, Cote GO (1989) J Electrochem Soc 136:356
6. Moshier WC, Davis GD, Ahearn JS, Hough HF (1987) J Electrochem Soc 134:2677
7. Davis GD, Moshier WC, Fritz TL, Cote GO (1990) J Electrochem Soc 137:422
8. Szklarska-Smialowska Z (1992) Corro Sci 33:1193
9. Inturi RB, Szklarska-Smialowska Z (1993) Corro Sci 34:705
10. Bockris JO'M, Minevski LV (1993) J Electroanal Chem Dateeee 349:375
11. Davis GD, Shaw BA, Rees BJ, Ferry M (1993) J Electrochem Soc 140:951
12. Davis GD, Shaw BA, Rees BJ, Pecile CA (1995) Surf Interf Anal 23:609
13. Zelenay P, Habib MA, Bockris JO'M (1984) J Electrochem Soc 131:2464
14. Zelenay P, Habib MA, Bockris JO'M (1986) Langmuir 2:393
15. Jovancicevic V, Bockris JO'M, Carbajal JL, Zelenay P, Mizuno T (1986) J Electrochem Soc 133:2219
16. Nagasubramanian G, Wheller BL, Hope GA, Bard AJ (1983) J Electrochem Soc 130:385
17. Peter LM (1984) In: Silva, AF (ed) Trends in interfacial electrochemistry. Ridel, Dordrecht, Holland, p 523
18. Chandrasekaran K, Bockris JO'M (1987) Electrochim Acta 32:1393
19. Azumi K, Ohtsuka T, Sato N (1987) J Electrochem Soc 134:1352
20. Kang Y (1997) PhD dissertation, Texas A&M University
21. Wagner CD, Riggs WM, Davis LE, Moulder JF, Muilenberg F. (eds) (1978) Handbook of X-ray photoelectron spectroscopy. Perkin-Elmer, Eden Prairie, Minn
22. Pleskov YV, Gurevich YY (1986) Semiconductors photoelectrochemistry. Plenum, New York, p 73
23. Furlong DN, Yates DE, Healy TW (1981) In: Trasatti S (ed) Electrodes of conductive metallic oxides. Elsevier, Amsterdam, p 367
24. Huang C, Stumm W (1973) J Colloid Interface Sci 43:409
25. Parks GA (1965) Chem Rev 65:177
26. Parks GA, Bruyn PL (1962) J Phys Chem 66:967
27. Natishan PM, McCafferty E, Hubler GK (1988) J Electrochem Soc 135:321
28. Kokarev GA, Kolesnikov VA, Gubin AF, Korobanov AA (1982) Electrochim 18:466
29. Marcus P, Herbelin JM (1993) Corro Sci 34:1123
30. Bockris JO'M, Khan SUM (1993) Surface Electrochemistry. Plenum, New York, p 90
31. Trasatti S (1984). In: Silva AF (ed) Trends in interfacial electrochemistry. Reidel, Dordrecht, p 25
32. Pleskov YV, Gurevich YY (1986) Semiconductor photoelectrochemistry. Plenum, New York, p 14
33. Butler MA, Ginley DS (1978) J Electrochem Soc 125:228
34. Frese KW (1979) J Vac Sci Technol 16:228
35. Nethercot AH (1974) Phys Rev Lett 33:1088
36. Poole RT, Williams DR, Riley JD, Jenkin JG, Liesegang J, Leckey RCG (1975) Chem Phys Lett 36:401
37. Bockris, JO'M, Gamboa-Aldeco M, Szklarczyk M (1992) J Electroanal Chem 339:355
38. Bockris JO'M, Jeng KT (1992) J Electroanal Chem 330:541
39. Barr TL (1977) J Vac Sci Technol 14:828
40. Alwitt RS (1976) In: Diggle JW, Vijh AK (eds) Oxides and Oxide Films, vol 4. Dekker, New York, p 169
41. Kono H, Kobayashi S, Takahashi H, Nagayama M (1980) Electrochim Acta 25:1667
42. Despic A, Parkhutic VP (1989) In: Bockris JO'M, White RE, Conway BE (eds) Modern aspects of electrochemistry, vol 20. Plenum, New York, p 401
43. Bernard WJ, Florio SM (1985) J Electrochem Soc 132:2319
44. Kobayashi M, Niioka Y (1990) Corro Sci 31:237
45. Robinson J, Thomson GE, Shimizu K (1994) In: Hebert KR, Thompson GE (eds) Oxide films on metals and alloys. The Electrochemical Society, Pennington, N.J., p 1
46. Frankel GS, Schrott AG, Davenport AJ, Isaacs HS, Jahnes CV, Russak MA (1994) J Electrochem Soc 141:83
47. Alwitt RS (1976) In: Diggle JW, Vijh AK (eds) Oxides and oxide films, vol 4, Dekker, New York, p 169
48. Catlow CRA (1981) In: Sorensen, OT (ed) Nonstoichiometric oxides. Academic, New York, p 61
49. Foley RT (1986) Corrosion 42:277
50. Bohni H (1987) In: Mansfeld F (ed) Corrosion mechanism, Dekker, New York, p 119
51. Richardson JA, Wood GC (1970) Corro Sci 10:313
52. Richardson JA, Wood GC (1973) J Electrochem Soc 120:193
53. Yahalom J, Poznansky Z (1978) In: Frankenthal RP, Kruger J (eds) Passivity of metals. Electrochemical Society, Princeton, p 1276
54. Vijh AK (1986) In: Bockris JO'M, Conway BE, and White RE (eds) Modern aspects of electrochemistry, vol 17. Plenum, New York, p 1
55. Smith E, Nabarro FRN (eds) (1979) Dislocations in solids, vol 4. North-Holland, New York, p 365
56. Wefers K (1990) In: Hart LD, Lense E (eds) Alumina chemicals: science and technology handbook. The American Ceramic Society, Westerville, Ohio, p 13
57. Mradt RC, Scott WD (1990) In: Hart LD, Lense E (eds) Alumina chemicals: science and technology handbook. The American Ceramic Society, Westerville, Ohio, p 23
58. Bockris JO'M, Beck W, Genshaw MA, Subramanyan PK, Williams FS (1971) Acta Metall 19:1209